Numerical Investigation of the Thermal Performance of an Axially Rotating Internally Finned Receiver Tube of a Parabolic Trough Concentrator

ANDREW S. TANIOUS[1, *], AHMED A. ABDEL-REHIM[1]
[1]The British University in Egypt
Department of Mechanical Engineering
Centre for Renewable Energy (CRE)
Suez Road, El Shoruok City, Cairo.
EGYPT

Abstract: Enhancement of the thermal performance of the parabolic trough receiver tube is one of the approaches to energy sustainability. In the present work, the thermal performance of an axially rotating receiver tube equipped with internal flat longitudinal fins is studied. The effects of both the fin height and the rate of axial rotation are investigated at low values of axial Reynold's number. The numerical analysis is held at various rotation rates using ANSYS Fluent.
The numerical findings showed that the effect of the axial rotation on the internally finned receiver tube is not significant yet negative where a maximum reduction of 6% in the outlet temperature is reached in the 2mm height internally finned tube at rotation rate of N=21. However, the analysis showed that as the rotation rate increases, the temperature homogeneity between the fluid layers also increases and thus the liquid stratification phenomenon between the fluid layers is eliminated. The percentage of temperature difference between the fluid layers near the pipe center and the layers near the pipe wall reaches an optimum value of 58.4% at N=21 which is confirmed by an optimum increase of 110% in Nusselt number at the same rotation rate. However, a maximum loss of 81.6% in pressure coefficient is found in the case of the 2mm internally finned tube due to the increased turbulence. Thus, the integration of pipe axial rotation and internal fins can yield an enhancement in the heat transfer to the parabolic trough concentrator receiver tube and thus its thermal performance.

*Keywords***:** Tube axial rotation, internal longitudinal fins, Flow in Parabolic Trough Receiver, Heat Transfer Enhancement, Swirl Flow, Concentrated Heat Flux.

Received: March 20, 2021. Revised: September 25, 2021. Accepted: October 7, 2021. Published: October 29, 2021.

Nomenclature:

Symbols		Greek Symbols	
V_r	Velocity in r-direction (m.s^{-1})	B	fraction of the liquid volume (K^{-1})
V_z	Velocity in z-direction (m.s^{-1})	μ	Dynamic viscosity (N.s.m^{-2})
V_Θ	Velocity in Θ-direction (m.s^{-1})	Θ	Transverse direction
R	Radial direction	Ω	Rotational velocity (rad.s^{-1})
Z	Axial direction	P	Fluid density (kg.m^{-3})
P	Pressure (Pa)	N	Kinematic viscosity (m^2.s^{-1})
T	Temperature (K)	Subscripts	
D	Internal diameter (m)	R	Radial component
Nu	Nusselt Number	Z	Axial component
Gr	Grashof Number	Θ	Angular component
q"	Heat flux density (W.m^{-2})	∞	Ambient condition
L	Pipe length (m)	G	Gravitational component
C_p	Specific heat at constant pressure (J.kg^{-1}.K^{-1})	Ω	Rotational component
K	Thermal conductivity (W. m^{-1}. K^{-1})	S	Surface
N	Rotation rate	A	Axial
Pr	Prandtl Number	M	Mean, average

1. Introduction

Solar power utilization is amongst the promising solution techniques to face serious energy issues such as the depletion of fossil fuels, the energy consumption increase, and global warming [1, 2]. The most common as well as most utilized concentrating solar technology is the parabolic trough concentrator (PTC) system [3]. The thermal performance of the parabolic trough is a serious issue that determines its feasibility and its further enhancement [3].

One of the most used techniques in the thermal performance enhancement of the parabolic trough receiver tubes is the usage of the internally finned tubes. Kursun [4] investigated the effect of using internal longitudinal flat as well as sinusoidal fins on the performance of the receiver tube of the parabolic trough collector. He found that the Nusselt number was enhanced by 25% for the flat fins and 78% for the sinusoidal ones at fluid inlet temperature (T_{in}=500K). He also found that decreasing T_{in} will increase Nu by (57-210%). In addition, Bellos et al. [5] examined the usage of the longitudinal internal fins inside a LS-2 receiver tube. They numerically investigated twelve different geometries for the fins with fin height ranging from 5mm to 20mm and fin thickness of 2mm to 6mm. they found that increasing the fin height and thickness resulted not only in higher thermal efficiency but also in higher pressure drop.

In continuation, Bellos et al. [6] numerically investigated the optimum number of internal longitudinal fins as well as their alignment that would lead to the optimum thermal performance of the receiver tube. The results showed that a total number of three fins located in the lower part of the tube at angles ($\beta=0^o$, $\beta=45^o$, and $\beta=315^o$) with respect to the negative y-axis yielded an optimum thermal efficiency of 68.59%. On the other hand, Munoz and Abanades [7] numerically analyzed using helical internal fins in the parabolic trough receiver tube. They investigated the effect of the number of fins as well as their helix angle on the thermal performance and pressure drop of the receiver tube. They found that using the optimum helix angle as well as the number of fins will lead to an optimum increase of 2% in the receiver thermal performance.

In continuation, Ahmed and Natarjan [8] numerically investigated the effect of using the toroidal rings on the thermal performance of LS-2 parabolic trough receiver tube. They examined nine cases of the toroidal rings with a diameter ratio of 0.88, 0.9, and 0.92 at three different pitch sizes of 2d, 3d, and 4d. They found that maximum thermal efficiency of 69.32% accompanied the usage of 0.88 diameter ratio and pitch size of 2d of toroidal rings. In addition, Ortiz et al. [9] thermally analyzed a solar tower finned receiver. Their results yielded a maximum thermal efficiency of 94.4% and the efficiency decreased with increasing the radiation and increased with increasing the mass flow rate.

The enhancement of the heat transfer rate can also be achieved by breaking the thermal boundary layer attached to the pipe surface through a mechanical aid [10]. Various applications made use of rotating tubes such as transmission shafts, turbomachinery, cyclone separators, rotors, and heating and/or cooling heat exchanger systems [11-13].

Seghir-Ouali et al. [14] investigated the heat transfer of an axially rotating pipe at various rotational speeds (4-800 rpm) to and from a circular pipe. They found that the heat transfer coefficient increased as a result of axial rotation. On the other hand, Gai et al. [15] studied the coefficient of heat transfer of the rotor cooling process in traction motors. The numerical results revealed that as the shaft's rotational speed increased, the heat transfer rate increased thus the shaft cooling rate also increased. Other improvements in heat transfer rate were reported by multiple researchers [16-19].

Morris and Rahmat-Abadi [20] investigated the combined effect of the internal fins and axial rotation on the heat transfer performance of the pipes. The results revealed that the secondary flow was obtained inside the pipe because of the Coriolis Effect that resulted from the axial rotation which enhanced the heat transfer rate. Wright et al. [21] investigated the effect of axial rotation of ducts equipped with variable rib geometries and the results showed that the W and V-shaped rib geometries yielded better results than other rib geometries in heat transfer rate enhancement despite their larger friction coefficient. In order to study the effect of insertions, Obed et al. [22] numerically investigated the effect of using a kenics mixer insertion in a rotating pipe. They found that as the rotation rate increased, the Nusselt number

decreased as the swirling motion resulted due to the existence of the kenics mixer began to diminish at higher rotation rates and was dominant at the lower rates.

From the previously mentioned studies, it has been noticed that using the internal fins in the parabolic trough receiver tubes would enhance the thermal performance of the PTC systems. In addition, using the axial rotation would enhance the rate of heat transfer to or from the rotating pipes at high rotation rates as well as uniform heat flux. However, up to the authors' knowledge, there is no published work that discussed the application of axial rotation in parabolic trough system internally finned receiver tubes where the heat flux is nonuniform as it is concentrated on a small portion in the bottom of the tube periphery as depicted in Fig.1. The rotational speeds used in this application should be kept at low levels because of the limitations of construction. The axial rotation can be used to redistribute the concentrated heat flux uniformly on the whole surface area of the pipe through alternating the portion of the pipe periphery exposed to the concentrated flux.
Accordingly, the present work will discuss the effect of axial rotation on heat transfer in the parabolic trough internally finned receiver tubes at low rotation rates with different fin heights numerically.

2. Physical Model

To study performance of an internally finned receiver tube of a parabolic trough concentrator system, a copper tube of length (L=1m), internal diameter (d_i=0.02m), and external diameter (d_o=0.022m) is used. Copper is chosen for its high thermal conductivity compared to other pipe materials. The tube is equipped with eight equally spaced flat longitudinal fins as shown in Fig.1 where each fin has a width of (W=1mm). Various fin heights of (H=0, 0.5, and 2mm) are considered.

A concentration ratio of (C=100x) of the direct solar radiation (1000 W/m^2) is assumed resulting in a concentrated heat flux of (100000 W/m^2) [23, 24]. Most of the concentrated radiation appears on (5-20%) of the bottom surface periphery of the tube and that's why the concentrated heat flux is applied to 10% of the bottom section of the tube [25, 26].

The working fluid is water with density (ρ), dynamic viscosity (μ), specific heat (Cp), and thermal conductivity (k) values are as follows: (ρ=998.2 kg/m^3, μ=0.00103 kg/m.s, Cp=4182 J/kg.K, and k=0.6 W/m.K).

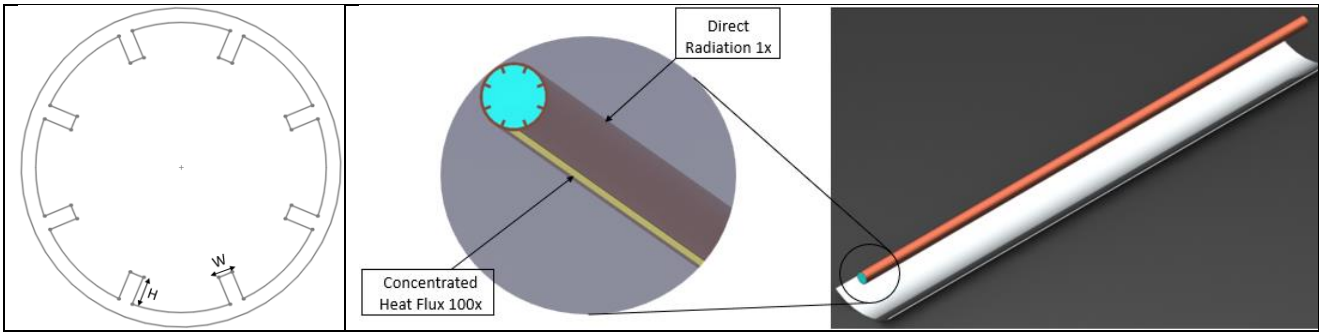

Figure 1:Schematic Model of the studied domain.

3. Mathematical Model

As the water enters the tube, it will encounter a tangential velocity component due to the wall rotation. This velocity will lead to proper mixing of the fluid layers between the center and the near-wall layers. The cold denser fluid layers located at the center start to move radially outward to replace the warmer less dense layers near the tube wall thus an enhanced temperature homogeneity will be resulted.

The Coriolis Effect interaction with the centrifugal acceleration affects the flow regime inside the tube and results in the secondary flow. The cylindrical coordinates (r,θ, and z) axes are used to represent the velocity components of this flow. The rotational motion will be represented with the aid of the radial velocity V_r, the transverse velocity V_Θ, and the axial velocity V_z. The tube angular velocity Ω is constant while it is exposed to a constant heat flux of 100000 W/m^2 applied on 10% of its lower half. The usage of the fins increases both the turbulence and the heat transfer to the fluid. The flow inside the tube is controlled by the following equations [27]:

Continuity Equation:

$$\frac{v_r}{r}+\frac{\partial v_r}{\partial r}+\frac{\partial v_z}{\partial z}+\frac{1}{r}\frac{\partial v_\theta}{\partial \theta}=0 \quad (1)$$

Momentum Equation:

r-component:

$$\rho\left(v_r\frac{\partial v_r}{\partial r}+\frac{v_\theta}{r}\frac{\partial v_r}{\partial \theta}-\frac{v_\theta^2}{r}+v_z\frac{\partial v_r}{\partial z}\right)=\rho g\beta(T-T_\infty)-\frac{\partial P}{\partial r}+\rho(\Omega^2 r+2\Omega v_\theta)\beta(T-T_\infty)+\mu\left(\frac{\partial^2 v_r}{\partial r^2}+\frac{1}{r}\frac{\partial v_r}{\partial r}-\frac{v_r}{r^2}+\frac{1}{r^2}\frac{\partial^2 v_r}{\partial \theta^2}-\frac{2}{r^2}\frac{\partial v_\theta}{\partial \theta}+\frac{\partial^2 v_z}{\partial z^2}\right) \quad (2)$$

θ-component:

$$\rho\left(v_r\frac{\partial v_\theta}{\partial r}+\frac{v_\theta}{r}\frac{\partial v_\theta}{\partial \theta}-\frac{v_r v_\theta}{r}+v_z\frac{\partial v_\theta}{\partial z}\right)=\frac{1}{r}\frac{\partial P}{\partial \theta}-2\rho\Omega v_r\beta(T-T_\infty)+\mu\left(\frac{\partial^2 v_\theta}{\partial r^2}+\frac{1}{r}\frac{\partial v_\theta}{\partial r}-\frac{v_\theta}{r^2}+\frac{1}{r^2}\frac{\partial^2 v_\theta}{\partial \theta^2}+\frac{2}{r^2}\frac{\partial v_r}{\partial \theta}+\frac{\partial^2 v_\theta}{\partial z^2}\right) \quad (3)$$

z-component:

$$\rho\left(v_r\frac{\partial v_z}{\partial r}+\frac{v_\theta}{r}\frac{\partial v_z}{\partial \theta}+v_z\frac{\partial v_z}{\partial z}\right)=-\frac{\partial P}{\partial z}+\mu\left(\frac{\partial^2 v_z}{\partial r^2}+\frac{1}{r}\frac{\partial v_z}{\partial r}+\frac{1}{r^2}\frac{\partial^2 v_z}{\partial \theta^2}+\frac{\partial^2 v_z}{\partial z^2}\right) \quad (4)$$

Energy Equation:

$$v_r\frac{\partial T}{\partial r}+\frac{v_\theta}{r}\frac{\partial T}{\partial \theta}+v_z\frac{\partial T}{\partial z}=\propto\left[\frac{\partial^2 T}{\partial r^2}+\frac{1}{r}\frac{\partial T}{\partial r}+\frac{1}{r^2}\frac{\partial^2 T}{\partial \theta^2}+\frac{\partial^2 T}{\partial z^2}\right] \quad (5)$$

Dimensionless parameters are used to solve these equations using ANSYS Fluent and shall be defined as:

$$v_r^*=\frac{v_r}{\frac{1}{2}\Omega D},\ v_\theta^*=\frac{v_\theta}{\frac{1}{2}\Omega D},\ v_z^*=\frac{v_z}{v_m},$$

$$r^*=\frac{r}{\frac{1}{2}D},\ z^*=\frac{z}{L},\ P^*=\frac{P}{\frac{1}{4}\rho\Omega^2 D^2},\ T^*=\frac{T-T_\infty}{T_s-T_\infty}$$

In order to solve the previous equations using FEM software, they should be rewritten in dimensionless form as follows:

r-component:

$$v_r^*\frac{\partial v_r^*}{\partial r^*}+\frac{v_\theta^*}{r^*}\frac{\partial v_r^*}{\partial \theta^*}-\frac{v_\theta^{*2}}{r^*}+\frac{1}{N(L/D)}v_z^*\frac{\partial v_r^*}{\partial z^*}=\frac{Gr_g}{Re_\Omega^2}T^*-\frac{\partial P^*}{\partial r^*}+(r^*+2V_\theta^*)\frac{Gr_\Omega}{Re_\Omega^2}T^*+\frac{4}{Re_\Omega}\left(\frac{\partial^2 v_r^*}{\partial r^{*2}}+\frac{1}{r^*}\frac{\partial v_r^*}{\partial r^*}-\frac{v_r^*}{r^{*2}}+\frac{1}{r^{*2}}\frac{\partial^2 v_r^*}{\partial \theta^{*2}}-\frac{2}{r^{*2}}\frac{\partial v_\theta^*}{\partial \theta^*}+\frac{1}{4(L/D)^2}\frac{\partial^2 v_r^*}{\partial z^{*2}}\right) \quad (6)$$

θ-component:

$$v_r^*\frac{\partial v_\theta^*}{\partial r^*}+\frac{v_\theta^*}{r^*}\frac{\partial v_\theta^*}{\partial \theta^*}-\frac{v_r^* v_\theta^*}{r^*}+\frac{1}{N(L/D)}v_z^*\frac{\partial v_\theta^*}{\partial z^*}=\frac{1}{r^*}\frac{\partial P^*}{\partial \theta^*}-2v_r^*\frac{Gr_\Omega}{Re_\Omega^2}T^*+\frac{4}{Re_\Omega}\left(\frac{\partial^2 v_\theta^*}{\partial r^{*2}}+\frac{1}{r^*}\frac{\partial v_\theta^*}{\partial r^*}-\frac{v_\theta^*}{r^{*2}}+\frac{1}{r^{*2}}\frac{\partial^2 v_\theta^*}{\partial \theta^{*2}}+\frac{2}{r^{*2}}\frac{\partial v_r^*}{\partial \theta^*}+\frac{1}{4(L/D)^2}\frac{\partial^2 v_\theta^*}{\partial z^{*2}}\right) \quad (7)$$

z-component:

$$v_r^*\frac{\partial v_z^*}{\partial r^*}+\frac{v_\theta^*}{r^*}\frac{\partial v_z^*}{\partial \theta^*}+\frac{1}{N(L/D)}\frac{\partial v_z^*}{\partial z^*}=\frac{-1}{4}\frac{N}{(L/D)}\frac{\partial P^*}{\partial z^*}+\frac{4}{Re_\Omega}\left(\frac{\partial^2 v_z^*}{\partial r^{*2}}+\frac{1}{r^*}\frac{\partial v_z^*}{\partial r^*}+\frac{1}{r^{*2}}\frac{\partial^2 v_z^*}{\partial \theta^{*2}}+\frac{1}{4(L/D)^2}\frac{\partial^2 v_z^*}{\partial z^{*2}}\right) \quad (8)$$

Energy Equation:

$$v_r^*\frac{\partial T^*}{\partial r^*}+\frac{v_\theta^*}{r^*}\frac{\partial T^*}{\partial \theta^*}+\frac{1}{N(L/D)}v_z^*\frac{\partial T^*}{\partial z^*}=\frac{4}{Re_\Omega Pr}\left(\frac{\partial^2 T^*}{\partial r^{*2}}+\frac{1}{r^*}\frac{\partial T^*}{\partial r^*}+\frac{1}{r^{*2}}\frac{\partial^2 T^*}{\partial \theta^{*2}}+\frac{1}{4(L/D)^2}\frac{\partial^2 T^*}{\partial z^{*2}}\right) \quad (9)$$

Thus, the following parameters would affect the flow in axially rotating tubes:

Rotational Reynold's Number: $Re_\Omega=\frac{\Omega D^2}{\nu}$

Axial Reynold's Number: $Re_a = \frac{v_m D}{\nu}$

Rate of rotation: $N = \frac{Re_\Omega}{Re_a}$

Rotational Grashof Number: $Gr_\Omega = \frac{\Omega^2 \beta (T_s - T_\infty) D^4}{\nu^2}$

Gravitational Grashof Number: $Gr_g = \frac{g \beta (T_s - T_\infty) D^3}{\nu^2}$

Prandtl Number: $Pr = \frac{Cp\ \mu}{k}$

And L/D is the aspect ratio.

Here in this study, the local Nusselt number is used to account for the heat transfer in the rotating pipe to the working fluid, where the following equation is used to calculate the average local Nusselt number:

$$Nu = \frac{q^{"} * D}{k(T_s - T_m)}$$

Where $q^{"}$ is the concentrated heat flux density in W/m^2, D is the tube internal diameter in m, k is the working fluid thermal conductivity in W/m.K, T_s is the pipe average surface temperature measured in K, and T_m is the average temperature of the working fluid in K [20].

4. Numerical Model

ANSYS Fluent software is used to solve the governing equations using finite element analysis (FEA). The analysis time is set to five consecutive minutes to let the solution be stabilized. The energy equation is used here to account for the heat transfer terms. The realizable k-Ɛ turbulence model is used and the enhanced wall treatment option is selected to detect the behavior of the near-wall thermal boundary layer precisely [22]. The mesh motion, as well as the frame motion, are used in the water pipe domain to account for the tube axial rotation while only the frame motion is activated for the water domain to model the fluid shear effect caused by the pipe wall on the fluid layers. The energy, turbulent dissipation rate Ɛ, turbulent kinetic energy k, and the momentum equations follow the second-order upwind convection scheme to achieve more accurate results. The pressure-velocity coupling follows the simple algorithm. The water density follows the Boussinesq model to account for the density variation with temperature. All the residuals should reach 10^{-6} for the convergence to occur to achieve accurate results.

A concentrated heat flux of (100000 W/m^2) which represents a concentration ratio of (C=100) is applied to the heating domain. The inlet temperature of the water is 300K and the gauge pressure is set to zero at the outlet boundary. In order to account for the shear effect between the pipe wall and the fluid layers, the no-slip moving wall is selected. The turbulence intensity used is 5%. A mass flow rate of 0.003 kg/s is selected as the mass flow rate of the working fluid in parabolic trough receiver tube should range from 0.001 to 0.025 kg/s according to Kumar et al. [28]. The effect of low rotation rates in the range [0-21] is investigated. The wall y+ value is kept under one which validates the usage of the realizable k- Ɛ with enhanced wall treatment turbulence model in this study.

A grid independence study is held for each case, the plain tube, the 0.5mm, and the 2mm internally finned tubes, to make sure that the results do not depend on the mesh size. Five different number of elements are tested for the plain tube and others are tested for each internally finned tube. The tested grid numbers for the plain tube are as follows: (184,450, 244,800, 313,650, 391,000, and 476,850). The observed variation in the average Nusselt number between (391,000 and 476,850) is less than 1%. In order to reduce the computational capacity and time, (391,000) number of elements is used as depicted in Fig.2. Figure 3 shows the final grid of this study.

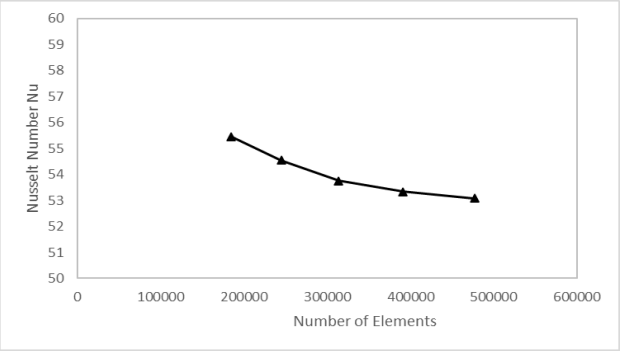

Figure 2: Grid Independence Study Results.

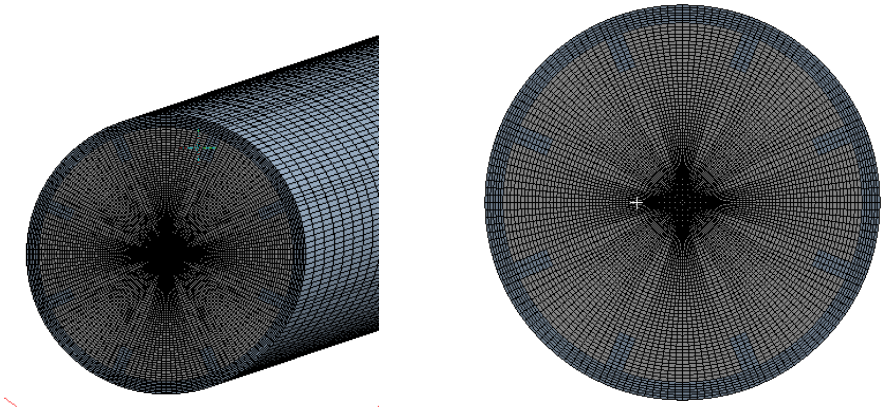

Figure 3: The structure of the final used grid

5. Results and Discussion

5.1. Numerical Model Validation

At first, the numerical model is validated by comparing the average local Nusselt number resulted from the numerical model of the plain tube at various rotation rates with the one resulted from the empirical correlation developed by Seghir-Ouali et al. [14] as shown in the following equation:

$$Nu = 0.01963Re_a^{0.9285} + 8.5101 * 10^{-6}Re_\Omega^{1.4513} \quad (11)$$

Where $0 < Re_a < 3 * 10^4$ and

$$1.6 < Re_\Omega < 2.77 * 10^5$$

The validation is held for the plain tube at an axial Reynold's number of 5000 and different rates of rotation as shown in Fig.4. The maximum error percentage observed between the numerical findings and the empirical correlation results is 4% which assures that a great agreement is found between the numerical and experimental results and that validates the numerical model accuracy.

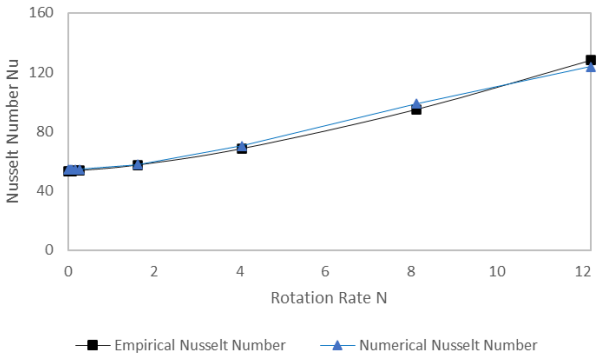

Figure 4: Validation of The Nusselt number numerical results (Re_a=5000).

5.2. Effect of fin height on the pipe thermal performance:

The numerical analysis indicates that as the fin height increases, the average local Nusselt number increases significantly. As the height increases from the plain tube to the 0.5mm height, the Nusselt number increases significantly where this increase reaches 12.6% in the 0.5mm height internally finned tube compared to the plain tube. As the fin height increases from 0.5mm to 2mm, the average local Nusselt number experiences a slight decrease of 1% which is insignificant as depicted in Fig.5.

The increase in the Nusselt number between the plain tube and the 0.5mm internally finned tube occurs due to the increase in the heat transfer rate to the working fluid which can be justified due to the increase in the surface area of the pipe in direct contact with the fluid as the fins can reach deeper areas in the fluid. On the other hand, the change is not significant between the 0.5mm and the 2mm internally finned tubes due to the increasing growth of the thermal boundary layer between the fins that works as a thermal insulation that reduces the rate of heat transfer to the inner fluid. Thus, the numerical analysis shows that using the internal fins enhances the thermal performance of the receiver tube, however, increasing the fin height could have a negative impact on the heat transfer rate to the receiver tube inner fluid as mentioned by Kursun [4].

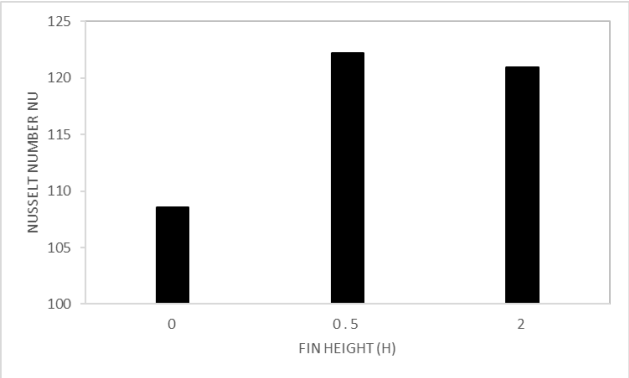

Figure 5:The average local Nusselt number of the receiver tube at different fin height.

5.3. Effect of rotational speed at different fin heights

The numerical findings show that the average outlet temperature of the water is not affected significantly by the axial pipe rotation either in the plain tube or in the internally finned tubes whereas the pipe rotation rate increases, the outlet temperature of the fluid does not increase significantly. They reveal that as the rate of rotation increases, the average outlet temperature experiences a slight decrease as shown in Fig.6. The maximum reduction in the average outlet temperature reaches 5% in the plain tube at rotation rate (N=21) where this maximum reduction reaches 6% in the 2mm height internally finned tube and 5.75% in the 0.5mm height internally finned tube at the same rotation rate (N=21).

This outlet temperature reduction is due to the increased growth of the thermal boundary layer at the low rates of rotation for the plain tube that works as an insulation layer reducing the heat transfer rate to the working fluid. However, as the rotation rate increases, the temperature gradient across the outlet boundary layer of the fluid domain decreases and that is due to the increased temperature homogeneity between the fluid layers and thus the enhanced mixing ratio between those layers as shown in Fig.7.

As for the internally finned tubes, at lower rotation rates, the ratio between the fluid layers entrapped between the longitudinal fins and the rest of the fluid increases, and those layers work as an insulation layer that holds the heat from reaching the fluid layers near the center of the pipe thus reducing the heat transfer rate from the pipe wall to the center of the fluid that's why the average outlet temperature of the water decreases. As the rate of rotation increases, the internal longitudinal fins break the thermal boundary layer thus increase the temperature homogeneity and the mixing ratio between the fluid layers as well. Figure 7 shows the temperature contours at the outlet boundary layer of both the plain tube and the internally finned tubes at different rotation rates.

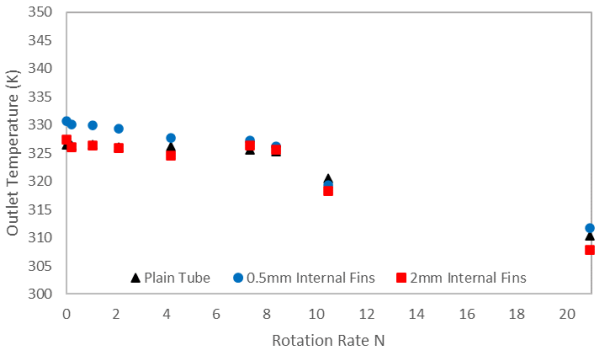

Figure 6: The Average outlet Temperature of the pipe at different rotation rates N.

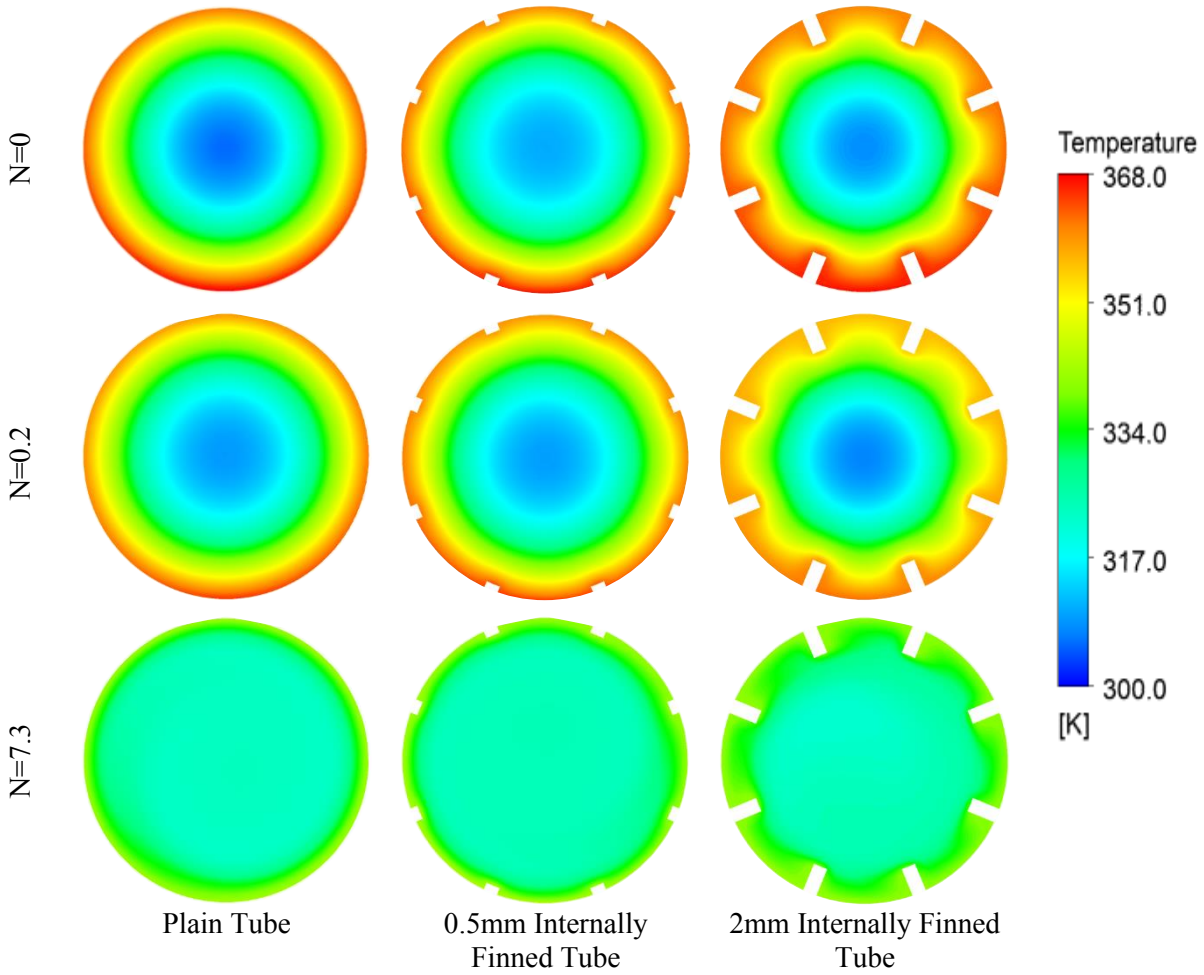

Figure 7:Temperature Contours of the pipe outlet at different rotation rates and pipe lengths.

Figure 7 shows the contours of temperature at the pipe outlet boundary for the plain pipe, 0.5mm, and 2mm internally finned tubes at rates of rotation N=0, N=0.2, and N=7.3. In case of the plain tube, as the rate of rotation increases, the temperature gradient across the outlet boundary decreases which means that enhanced fluid mixing occurs as can be seen from Fig.7. As for the internally finned tubes, the same phenomenon can be seen; however, the growth of a thermal boundary layer due to the entrapped fluid between the fins increases, and this layer acts as a thermal insulator that prevents the heat from reaching the pipe center.

A comparison is conducted between the fluid bulk temperature along the pipe, the average fluid temperature at the pipe centerline, and the average wall temperature of the pipe to detect the gradient of temperature across the pipe length and to understand the effect of the pipe axial rotation on the mixing ratio between the fluid layers. The temperature difference between the fluid center, the pipe wall, and the fluid bulk temperature for the plain tube is shown in Fig. 8(a).

It can be noticed that for the plain tube, as the rate of rotation increases, the temperature difference gap value between the fluid center and the pipe wall temperatures decreases which indicates that the mixing ratio between the fluid layers is enhanced. The difference in temperature reaches an optimum value of 48.4% at a rate of rotation of N=8.4 in comparison with the stationary pipe.

For the case of the 0.5mm internally finned tube, this temperature difference decreases as the rotation rate increases reaching a maximum reduction value of 46% at a rotation rate of N=10.5 when compared to the stationary tube as can be seen in Fig. 8(b).

In the case of the 2mm internally finned tube, the same phenomenon is noticed where an optimum reduction of 58.4% can be achieved at a rotation rate of N=21 compared to the stationary tube as depicted in Fig.8(c).

As the fins' height is increased, the percentage of temperature reduction between the pipe wall and the fluid inner layers increases leading to better fluid mixing and better temperature homogeneity across the pipe cross-section. This temperature reduction also indicates that the heat transfer rate from the pipe wall to the inner fluid layers is enhanced. This indicates that better thermal performance and thus enhanced heat transfer rates can be reached at larger pipe lengths.

The enhanced mixing ratio between the fluid layers causes a decrease in the local liquid stratification phenomenon which might happen because of the variation in density between the fluid layers [29]. The variation in temperature between the fluid layers leads to this variation in density which causes liquid stratification. Thus, the mixing ratio enhancement leads to improvement in temperature homogeneity.

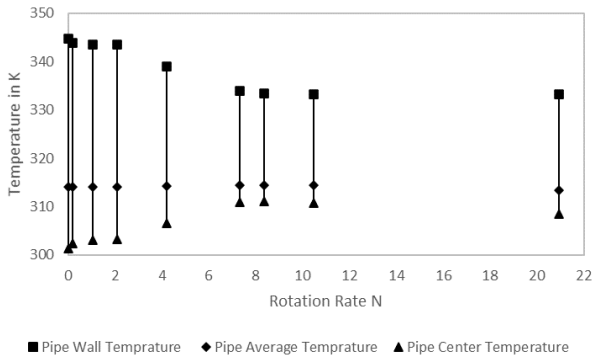

(8-A)

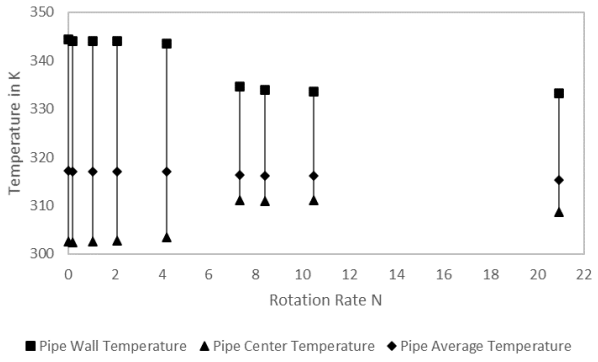

(8-B)

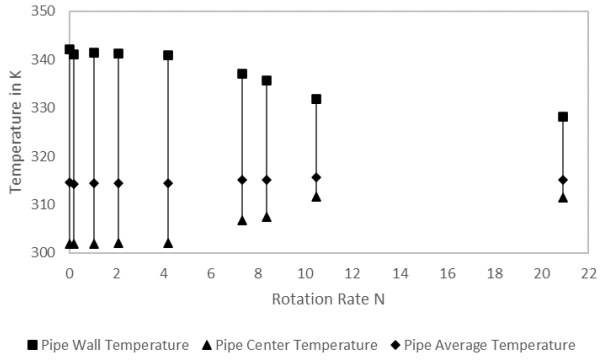

(8-C)

Figure 8: Average Temperature Difference at different rotation rates for: a) Plain tube, b) 0.5mm internally finned tube and c) 2mm internally finned tube.

The numerical findings indicates that as the rate of rotation increases, the average local Nusselt number in the tube also increases. For the plain tube, at the low rates of rotation (N=0-2.1), the rate of increase in Nusselt number is not significant while at higher rotation rates (N=2.1-7.3), the rate of increase in Nusselt number is higher. A maximum increase of 62.8% in the Nusselt number can be reached at a rotation rate of N=10.5 for the plain tube case when compared to the stationary one. It is also noticed that the Nusselt number slightly decreases at rotation rates (N=10.5-21) as can be seen in Fig.9.

As for the 0.5mm internally finned tube, The average local Nusselt number across the tube is almost constant at lower rotation rates (N=0-4.2) while the rate of increase in Nusselt number began to grow suddenly at rotation rate (N=4.2) where the Nusselt number continued to increase rapidly till a rotation rate of (N=8.4) is reached where a maximum increase of 55.6% is achieved in Nusselt number at rotation rate (N=10.5) compared to its stationary pipe. The Nusselt number then experiences a slight decrease at higher rotation rates (N=10.5-21) as depicted in Fig.9.

The same trend is obtained in the case of the 2mm internally finned tube where the Nusselt number is constant at the low rotation rates (N=0-4.2). The Nusselt number then increases with increasing the rotation rate where a maximum increase of 110% is obtained at rotation rate (N=21) compared to its stationary pipe as shown in Fig.9.

It is clear that as the fin height increases, the Nusselt number increases at the same rotation rate. This can be justified by the ability of the fin to reach deeper layers of fluid near the pipe center as its height

increases that will increase the amount of heat transferred to the center layers of the fluid causing an increase in the average temperature of the water along with the heat capacity resulting in an increase in the Nusselt number which indicates the enhanced rate of heat transfer to the working fluid inside the pipe.

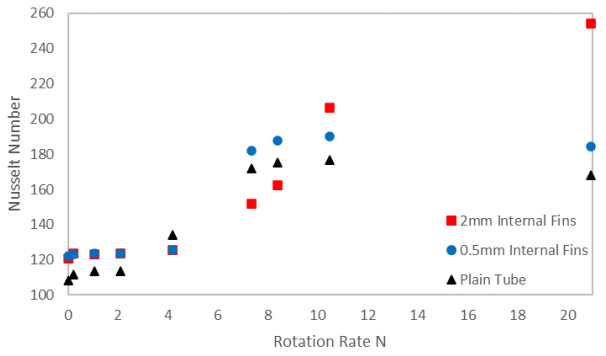

Figure 9: The average local Nusselt number at various rotation rates.

5.4. Effect of using internal fins on pressure losses

The numerical findings reveal that as the rate of rotation increases, the loss in pressure coefficient also increases which indicates that the pressure drop increases. At low rotation rates (N=0-7.3), the increasing losses in pressure coefficient in the three cases are insignificant. The losses in pressure coefficients for both the plain and the 0.5mm height internally finned tubes are almost the same, however; for the 2mm internally finned tube, the losses are higher. As the rate of rotation increases from (N=7.3-20.5), the losses in the pressure coefficients also increase where the rate of their increase in the case of the 2mm height internally finned tube is much higher than the other two cases as can be seen in Fig.10.

The maximum increases in losses in the pressure coefficients in the plain tube, 0.5mm, and the 2mm height internally finned tubes are 59.9%, 61.8%, and 81.6% respectively compared to their stationary tubes. These large increases in the losses in pressure coefficient occur due to the turbulence increase because of the combined effect of the axial pipe rotation along with the internal fins.

Figure 11 displays the velocity surface streamlines at the outlet cross-section of plain tube, 0.5 mm and 2mm height internally finned tube. As can be seen in Fig.11, increasing the rotation rate increases the vortices in the pipe thus increasing the turbulence in the pipe. In addition, increasing the fin height also increases the vortices between the fins thus increasing the turbulence inside the pipe and that's why the pressure drop increases.

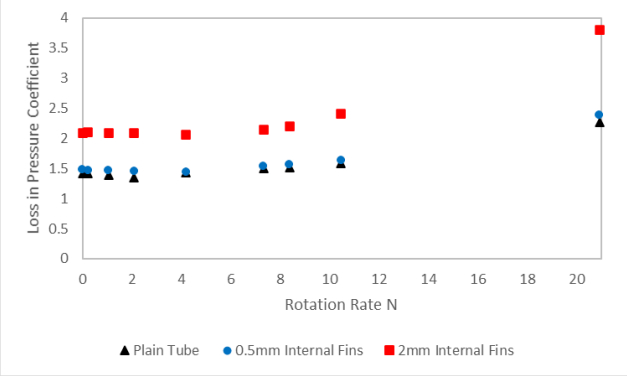

Figure 10: Pressure coefficient losses at various rotation rates.

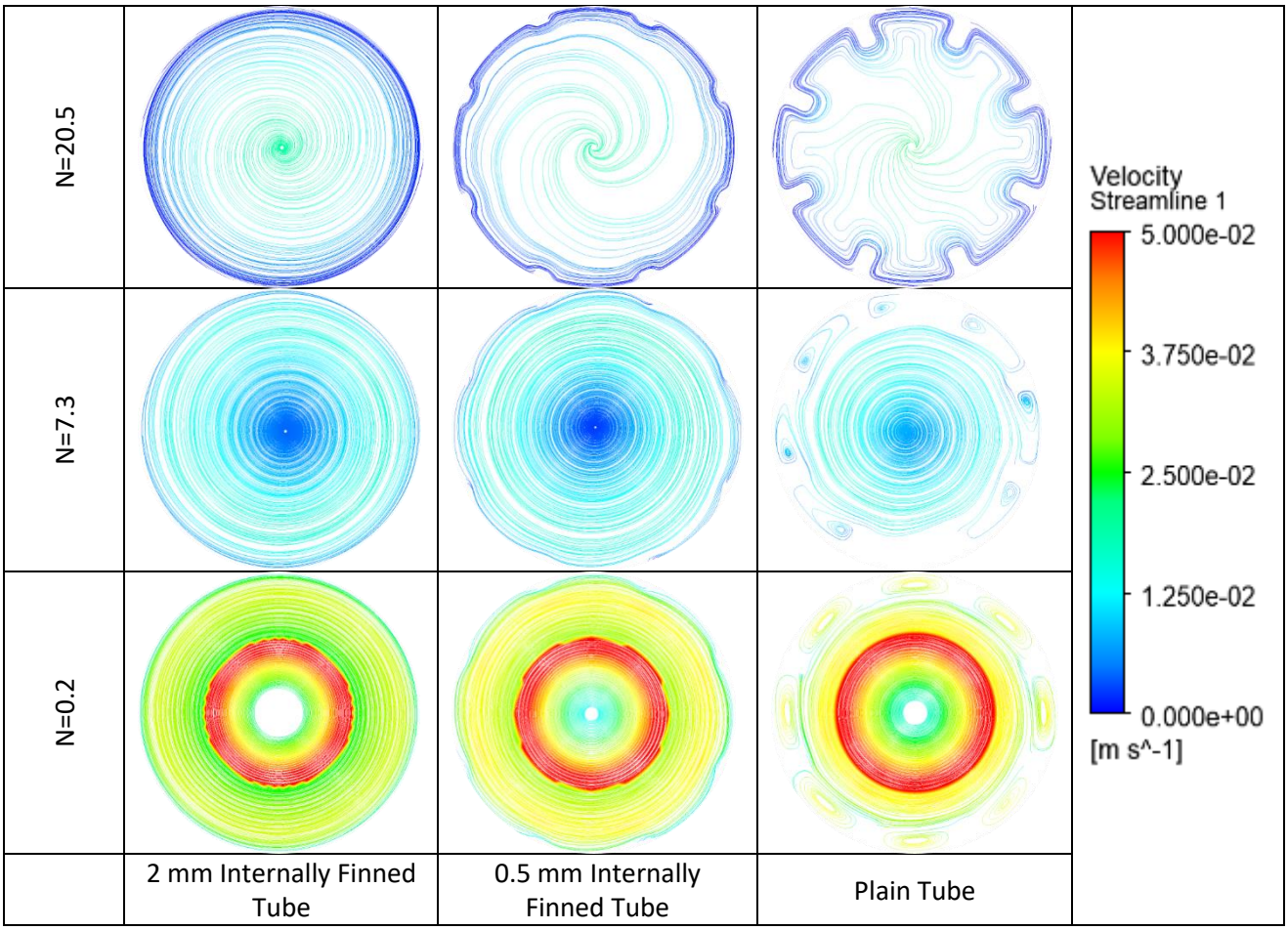

Figure 11:Velocity surface streamlines at the outlet cross-section of the pipes at different rates of rotation.

6. Conclusion

The thermal performance of an axially rotating receiver tube of a parabolic trough system equipped with internal longitudinal flat fins is studied numerically using ANSYS Fluent. The effect of using internal fins along with axial rotation on the heat transfer rate to a parabolic trough receiver tube at low axial Reynold's number for a 1-meter tube is investigated. The numerical findings indicate that the axial rotation has an insignificant yet negative impact on the outlet temperature of the working fluid. As the rotation rate increases, the outlet temperature of the working fluid slightly decreases in both the plain tube and the internally finned ones. This decrease in the outlet temperature occurs due to the increasing growth of a thermal boundary layer attached to the inner surface of the pipe at low rotation rates which acts as an insulation layer that holds the heat from reaching the center layers of the fluid. In addition, in the internally finned tubes, the fluid layers entrapped between the fins also act as an insulation layer.

It is noticed that as the rate of rotation increases, the difference between the pipe wall temperature and the fluid center temperature decreases significantly across the pipe length thus the local liquid stratification decreases and thus at larger pipe lengths, an enhanced heat transfer can be obtained as the amount of heat transfer to the fluid will be larger. Also, as the fin height increases, this temperature difference decreases and that is because the fin can transfer heat from the pipe surface to deeper areas towards the center of the pipe and increases the rate of heat transfer to the working fluid.

The numerical results showed that with the increase of the rotation rate, the Nusselt number also increases where a maximum increase of 62.8%, 55.6%, and 110% is obtained for the plain tube, 0.5mm, 2mm internally finned tubes respectively compared to the stationary pipe in each case.

This increase in the Nusselt number is higher at the larger fin height of 2mm which indicates that the larger the fin height, the better enhancement happens to the Nusselt number. However, The losses in

pressure coefficient show an increase of 59.9%, 61.8%, and 81.6% for the plain tube, 0.5mm, and 2mm height internally finned tubes which is justified because of the increased turbulence ration due to the usage of both the pipe axial rotation and the internal fins. The integration of the axial pipe rotation with the internal fins in the parabolic trough receiver pipe yields an enhancement in the heat transfer to the working fluid inside the pipe thus enhancing the thermal performance of the receiver tube of the parabolic trough solar concentrator.

References:

[1] Rogada, J.R.; Barcia, L.A.; Martinez, J.A.; Menendez, M.; Juez, F.J.D. Comparative Modeling of a Parabolic Trough Collectors Solar Power Plant with MARS Models. Energies **2018**, 11, 37.

[2] Praveen, R.P.; Baseer, M.A.; Awan, A.B.; Zubair, M. Performance Analysis and Optimization of a Parabolic Trough Solar Power Plant in the Middle East Region. Energies 2018, 11, 741.

[3] Bellos, E., & Tzivanidis, C. (2018). Enhancing the Performance of Evacuated and Non-Evacuated Parabolic Trough Collectors Using Twisted Tape Inserts, Perforated Plate Inserts, and Internally Finned Absorber. Energies, 11(5), 1129. https://doi.org/10.3390/en11051129

[4] Kurşun, B. (2019). Thermal performance assessment of internal longitudinal fins with sinusoidal lateral surfaces in parabolic trough receiver tubes. *Renewable Energy*, *140*, 816–827. https://doi.org/10.1016/j.renene.2019.03.106

[5] Bellos, E., Tzivanidis, C., & Tsimpoukis, D. (2017). Thermal enhancement of parabolic trough collector with internally finned absorbers. Solar Energy, 157, 514–531. https://doi.org/10.1016/j.solener.2017.08.067.

[6] Bellos, E., Tzivanidis, C., & Tsimpoukis, D. (2018). Optimum number of internal fins in parabolic trough collectors. Applied Thermal Engineering, 137, 669–677.https://doi.org/10.1016/j.applthermaleng.2018.04.037.

[7] Muñoz, J., & Abánades, A. (2011). Analysis of internal helically finned tubes for parabolic trough design by CFD tools. Applied Energy, 88(11), 4139–4149. https://doi.org/10.1016/j.apenergy.2011.04.026.

[8] Arshad Ahmed, K., & Natarajan, E. (2019). Thermal performance enhancement in a parabolic trough receiver tube with internal toroidal rings: A numerical investigation. Applied Thermal Engineering, 162, 114224. https://doi.org/10.1016/j.applthermaleng.2019.114224.

[9] Reddy, V. S., Kaushik, S. C., & Tyagi, S. K. (2013). Exergetic analysis and economic evaluation of central tower receiver solar thermal power plant. International Journal of Energy Research, 38(10), 1288–1303. https://doi.org/10.1002/er.3138.

[10] Alam, T., & Kim, M.-H. (2017, August 31). A comprehensive review on single phase heat transfer enhancement. Renewable and Sustainable Energy Reviews, 81, 813-839. doi:10.1016.

[11] M. Ould-Rouiss, A. Dries, A. Mazouz, Numerical predictions of turbulent heat transfer for airflow in rotating pipe, Int. J. Heat Fluid Flow 31 (4) (2010) 507–517.

[12] K. Nishibori, K. Kikuyama, M. Murakami, Laminarization of turbulent flow in the inlet region of an axially rotating pipe: fluids engineering, JSME International Journal 30 (260) (1987) 255–262.

[13] J. Davis, S. Ganju, A. Venkatesh, N. Ashton, S.C. Bailey, C. Brehm, Coherence analysis of rotating turbulent pipe flow, in: AIAA Scitech 2020 Forum, 2020, p. 1570.

[14] S. Seghir-Ouali, D. Saury, S. Harmand, O. Phillipart, D. Laloy, Convective heat transfer inside a rotating cylinder with an axial airflow, Int. J. Therm. Sci. 45 (12) (2006) 1166–1178.

[15] Y. Gai, M. Kimiabeigi, Y.C. Chong, J.D. Widmer, J. Goss, U. SanAndres, D.A. Staton, On the measurement and modeling of the heat transfer coefficient of a hollow-shaft rotary cooling system for a traction motor, IEEE Trans. Ind. Appl. 54 (6) (2018) 5978–5987.

[16] J.F. Humphreys, W.D. Morris, H. Barrow, Convection heat transfer in the entry region of a tube which revolves about an axis parallel to itself, Int. J. Heat Mass Tran. 10 (3) (1967) 333–340.

[17] G. Luca Basso, Improved Thermal Models for Predicting End Winding Heat Transfer, Master's Thesis, KTH Royal Institute of Technology), 2017.

[18] Y.C. Chong, Thermal Analysis and Airflow Modeling of Electrical Machines, Doctoral dissertation, University of Edinburgh, 2015.

[19] O.Y. Abotsi, J.P. Kizito, Heat transfer enhancement in an axially rotating pipe with twisted tape insert, Am. J. Mech. Eng. 8 (1) (2020) 1–8.

[20] Moriss WD, Rahmat-Abadi KF. Convective heat transfer in rotating ribbed tubes. Int J Heat Mass Transfer 1996; 39:2253–66.

[21] Wright LM, Fu WL, Han JC. Thermal performance of angled, V-shaped, and W-shaped rib turbulators in rotating rectangular cooling channels (AR = 4:1). J Turbomach 2004; 126:604–14.

[22] Abotsi, O. Y., & Kizito, J. P. (2020). Turbulent heat transfer enhancement in an axially rotating pipe fitted with kenics segment mixer. Results in Engineering, 7, 100146-100152. doi: 10.1016/j.rineng.2020.100146

[23] Mwesigye, A., & Yılmaz, İ H. (2020). Thermal and thermodynamic benchmarking of liquid heat transfer fluids in a high concentration ratio parabolic trough solar collector system. Journal of Molecular Liquids, 319, 114151. doi: 10.1016/j.molliq.2020.114151.

[24] Breeze, P. (2016). Chapter 4 - Parabolic Trough and Fresnel Reflector Solar Power Plants. In 1358705014 994338852 P. Breeze (Author), Solar power generation (pp. 25-34). Amsterdam, Netherlands: Academic Press. doi:10.1016/B978-0-12-804004-1.00004-X

[25] Peng, W., Hussein, E., & Sadaghiani, O. K. (2021). Evaluation of heat Flux distribution Uniformity around the RECEIVER tube of parabolic Trough collector based on SIX statistical and geometrical indices. International Journal of Heat and Mass Transfer, 164, 120547. doi: 10.1016/j.ijheatmasstransfer.2020.120547.

[26] Mwesigye, A., Bello-Ochende, T., & Meyer, J. P. (2014). Minimum entropy generation due to heat transfer and fluid friction in a parabolic trough receiver with non-uniform heat flux at different rim angles and concentration ratios. Energy, 73, 606-617. doi: 10.1016/j.energy.2014.06.063.

[27] Abotsi, O. Y., & Kizito, J. (2020). Numerical study of heat transfer augmentation in an Axially Rotating Pipe equipped with Kenics mixer. Case Studies in Thermal Engineering, 21, 100695100702.doi:10.1016/j.csite.2020.100695.

[28] Devander Kumar & Sudhir Kumar (2018) Thermal performance of the solar parabolic trough collector at different flow rates: an experimental study, International Journal of Ambient Energy, 39:1, 93-102, DOI: 10.1080/01430750.2016.1269673

[29] Abed, N., & Afgan, I. (2020). An extensive review of various technologies for enhancing the thermal and optical performances of parabolic trough collectors. International Journal of Energy Research, 44(7), 5117-5164. doi:10.1002/er.5271

Contribution of individual authors to the creation of a scientific article

Andrew S. Tanious carried out the simulations and the numerical analysis, developed the enhancement modification idea, developed the numerical model, and wrote the research article.

Ahmed A. Abdel-Rehim got the enhancement modification idea, revised the paper, and supervised the simulation and the numerical analysis and justified the numerical result.